Cellular/Molecular

The Serotonergic Dorsal Raphe Promotes Emergence from Propofol Anesthesia in Zebrafish

Xiaoxuan Yang,[1*] Shan Zhu,[1*] Miaoyun Xia,[1*] Le Sun,[2] Sha Li,[2,3] Peishan Xiang,[2] Funing Li,[2] Qiusui Deng,[2,4] Lijun Chen,[2,3] Wei Zhang,[2] Ying Wang,[1] Qiang Li,[1] Zhuochen Lyu,[1] Xufei Du,[2] Jiulin Du,[2,3] Qianzi Yang,[1] and Yan Luo[1]

[1]Department of Anesthesiology, Ruijin Hospital, Shanghai Jiao Tong University School of Medicine, Shanghai 200025, China, [2]Institute of Neuroscience, State Key Laboratory of Neuroscience, Center for Excellence in Brain Science and Intelligence Technology, Chinese Academy of Sciences, Shanghai 200031, China, [3]School of Life Science and Technology, ShanghaiTech University, Shanghai 201210, China, and [4]University of Chinese Academy of Sciences, Beijing 100049, China

The mechanisms through which general anesthetics induce loss of consciousness remain unclear. Previous studies have suggested that dorsal raphe nucleus serotonergic ($DRN^{5\text{-}HT}$) neurons are involved in inhalational anesthesia, but the underlying neuronal and synaptic mechanisms are not well understood. In this study, we investigated the role of $DRN^{5\text{-}HT}$ neurons in propofol-induced anesthesia in larval zebrafish (sex undetermined at this developmental stage) using a combination of in vivo single-cell calcium imaging, two-photon laser ablation, optogenetic activation, in vivo glutamate imaging, and in vivo whole-cell recording. We found that calcium activity of $DRN^{5\text{-}HT}$ neurons reversibly decreased during propofol perfusion. Ablation of $DRN^{5\text{-}HT}$ neurons prolonged emergence from 30 μM propofol anesthesia, while induction times were not affected under concentrations of 1, 3, and 30 μM. Additionally, optogenetic activation of $DRN^{5\text{-}HT}$ neurons strongly promoted emergence from propofol anesthesia. Propofol application to $DRN^{5\text{-}HT}$ neurons suppressed both spontaneous and current injection-evoked spike firing, abolished spontaneous excitatory postsynaptic currents, and decreased membrane input resistance. Presynaptic glutamate release events in $DRN^{5\text{-}HT}$ neurons were also abolished by propofol. Furthermore, the hyperpolarization of $DRN^{5\text{-}HT}$ neurons caused by propofol was abolished by picrotoxin, a $GABA_A$ receptor antagonist, which shortened emergence time from propofol anesthesia when locally applied to the DRN. Our results reveal that $DRN^{5\text{-}HT}$ neurons in zebrafish are involved in the emergence from propofol anesthesia by inhibiting presynaptic excitatory glutamate inputs and inducing $GABA_A$ receptor-mediated hyperpolarization.

Key words: 5-HT; dorsal raphe; general anesthesia; propofol; zebrafish

Significance Statement

The neural mechanisms of general anesthesia (GA) remain unclear. We studied the role of the dorsal raphe nucleus serotonergic ($DRN^{5\text{-}HT}$) neurons in propofol anesthesia using larval zebrafish, employing in vivo calcium imaging at single-neuron resolution, two-photon ablation, optogenetic activation, and in vivo whole-cell recording. We found that the $DRN^{5\text{-}HT}$ neurons are involved in emergence from anesthesia, but not induction. Propofol suppresses $DRN^{5\text{-}HT}$ activity by inhibiting the activity of $DRN^{5\text{-}HT}$ neurons via $GABA_A$ receptors and blocking presynaptic excitatory glutamate inputs. These findings further support larval zebrafish as an ideal model for investigating the mechanisms of GA.

Introduction

The discovery of general anesthetics has revolutionized surgical procedures in medicine over the past centuries (Robinson and Toledo, 2012; Jiang-Xie et al., 2019). Over 300 million surgeries are performed worldwide each year, with a projected minimum operative volume of 5,000 surgical procedures per 100,000 population by 2030 (Meara et al., 2015). Previous studies exploring the mechanisms of general anesthesia (GA) have mainly focused

Received Nov. 7, 2023; revised Dec. 30, 2024; accepted Jan. 27, 2025.

Author contributions: X.Y., J.D., Q.Y., and Y.L. designed research; X.Y., S.Z., L.S., S.L., P.X., and M.X. performed research; F.L., Q.D., L.C., W.Z., and X.D. contributed unpublished reagents/analytic tools; Q.L., Z.L., and Y.W. analyzed data; X.Y., Q.Y., and Y.L. wrote the paper.

This work was supported by the National Natural Science Foundation of China (82001451 to X.Y., T2293734 and T2293730 to Y.L., 82271285 to Q.Y.). We appreciate Yongxin Yang for the expert assistance with the in vivo whole-cell recording technique and Changmei Zhang for the suggestions on writing the manuscript. All mentioned individuals are members of Jinlin Du's lab. We also thank Professor Zhe Zhang, Ph.D., from Institute of Neuroscience, State Key Laboratory of Neuroscience, Center for Excellence in Brain Science and Intelligence Technology, Chinese Academy of Sciences, for providing tetrodotoxin samples in electrophysiology experiment.

*X.Y., S.Z., and M.X. contributed equally to this work.

The authors declare no competing financial interests.

Correspondence should be addressed to Yan Luo at ly11087@rjh.com.cn or Qianzi Yang at qianziyang@hotmail.com.

https://doi.org/10.1523/JNEUROSCI.2125-23.2025

on molecular targets such as $GABA_A$ receptors, *N*-methyl-D-aspartate (NMDA) receptors, two-pore-domain potassium channels, and hyperpolarization-activated cyclic nucleotide-gated (HCN) channels (Hemmings et al., 2005). However, the synaptic mechanisms that enable GA to produce unconsciousness remain poorly understood.

Sleep serves as a useful metaphor for clinical anesthesiologists to explain GA to surgical patients, as both share similar traits of reversible unconsciousness and EEG patterns (Brown et al., 2010). Exploring the overlapping mechanisms between GA and sleep provides a novel way to understand how GA induces unconsciousness (Franks, 2008). Several sleep–wake-related neural circuits have been reported to participate in the induction or emergence of GA, including cholinergic and orexinergic neurons from the basal forebrain (Luo et al., 2020; Wang et al., 2021), dopamine and GABAergic neurons from the ventral tegmental area (Yin et al., 2019; Qiu et al., 2020), neurons expressing dopamine receptors from the nucleus accumbens (Zhang et al., 2021), tachykinin 1 neurons of the ventrolateral preoptic nucleus (Reitz et al., 2021) histaminergic neurons of the tuberomammillary nucleus (Luo and Leung, 2011), norepinephrine and orexinergic neurons of the locus ceruleus (Du et al., 2018; Wang et al., 2021), glutamatergic neurons of the parabrachial nucleus (Melonakos et al., 2021) and paraventricular thalamus (S. Ren et al., 2018), etc.

Serotonin (5-HT), a neurotransmitter involved in regulating various brain functions like depression and cognition, has long been implicated in the regulation of sleep and wakefulness, providing dominant projections to the midbrain and forebrain, and being innervated by the cerebral cortex, limbic systems, basal forebrain, and hypothalamus (J. Ren et al., 2018). Destruction of serotonergic areas in the brainstem decreases the minimum alveolar concentration of halothane and cyclopropane (Roizen et al., 1978). Isoflurane anesthesia decreases the release of 5-HT in the frontal cortex of rats (Mukaida et al., 2007), and activation of 5-HT neurons in the dorsal raphe nucleus (DRN) promotes arousal from isoflurane anesthesia (Li et al., 2021). While these studies suggest the potential contribution of $DRN^{5\text{-}HT}$ neurons to inhalational anesthesia, the understanding of its role in intravenous anesthesia and its exact synaptic mechanisms are very limited. Unlike inhalational anesthetics, which have a wide range of molecular targets (Hemmings et al., 2019), propofol, the most widely used intravenous anesthetic, primarily targets $GABA_A$ receptors (Franks, 2008). Therefore, propofol provides a good model for exploring the mechanisms of synaptic transmission of general anesthetics in specific neurons through a single type of molecular target.

Considering that zebrafish larvae possess an evolutionarily conserved central nervous system that is highly approachable in intact animals for in vivo electrophysiological recording and lacks the complex behavioral repertoire of murine systems that can confound interpretation of the serotonergic system (Oikonomou et al., 2019), we used larval zebrafish as the model in the current study. Mammalian genes for 19 subunit isotypes of $GABA_A$ receptors have been identified (α1–6, β1–3, γ1–3, δ, ε, θ, π, and ρ1–3), and most neuronal $GABA_A$ receptors contain two α subunits and two β subunits along with γ, δ, or another β subunit (Olsen and Sieghart, 2009). It is reported that global and pan-neuronal β3−/− mice and zebrafish are selectively insensitive to propofol, indicating phylogenetic conservation of $GABA_A$ receptors as anesthetic targets (Quinlan et al., 1998; Yang et al., 2019). Specifically, we hypothesize that propofol exerts some of its anesthetic effects through $GABA_A$ receptors in the $DRN^{5\text{-}HT}$ system.

We performed in vivo calcium imaging at single-cell resolution to detect the influence of propofol on $DRN^{5\text{-}HT}$ neurons. Specific two-photon ablation and optogenetic activation were used to manipulate $DRN^{5\text{-}HT}$ neurons and illustrate their role in the induction and emergence processes of propofol-induced GA. Finally, the mechanisms were explored by in vivo whole-cell recording and in vivo glutamate imaging.

Materials and Methods

Zebrafish. Details of the resources and zebrafish strains used are provided in Tables 1 and 2, respectively. Zebrafish (*Danio rerio*) were used with approval from the Institute of Neuroscience, Chinese Academy of Sciences. All experiments were performed on larvae at 6–7 d postfertilization (dpf). Sex has not been determined at this stage of development. Embryos and larvae were housed in Petri dishes (~17 cm diameter) containing Hank's solution (in mM: 140 NaCl, 5.4 KCl, 0.25 Na_2HPO_4, 0.44 KH_2PO_4, 1.3 $CaCl_2$, 1.0 $MgSO_4$, and 4.2 $NaHCO_3$), pH 7.2, and placed in an incubator at 28.5°C under a 14/10 h light/dark cycle for incubation and culture.

All zebrafish lines were derived from the nacre strain. *Ki(tph2:GAL4FF, cmlc2:EGFP)* lines were crossed with different UAS lines to express various target genes through the GAL4-UAS system, such as *Tg(UAS:GCaMP6s)* for in vivo calcium imaging, *Tg(UAS:ChrimsonR-mKate)* for optogenetic activation, and *Tg(UAS:lyn-tdTomato)* for in vivo whole-cell recording. The *Ki(tph2:EGFP)* line was used for two-photon laser lesion.

To express the intensity-based glutamate–sensing fluorescent reporter (iGlusnFR3) in $DRN^{5\text{-}HT}$ neurons, embryos of the *Ki(tph2:GAL4FF, cmlc2:EGFP)* mutant line were injected at the one-cell stage with 25 ng/μl plasmid DNA encoding iGluSnFR3 and 25 ng/μl Tol2 transposase mRNA diluted in ddH_2O with 0.025% phenol red (Aggarwal et al., 2023). Tol2 sequences flanking the expression cassettes allowed for stable genomic integration.

In vivo cellular-resolution imaging. To conduct in vivo cellular-resolution calcium and glutamate imaging, *Ki(tph2:GAL4FF,cmlc:EGFP);Tg(UAS:GCaMP6s)* and *Ki(tph2:GAL4FF,cmlc2:EGFP); Tg(UAS:iGluSnFR3)* larvae, respectively, were embedded dorsal side up in 1.5% low-melting agarose in a glass-bottom dish at 6–7 dpf. They were imaged

Table 1. Key resources

Reagent or resource	Source	Identifier
Chemicals		
α-Bungarotoxin	Tocris Bioscience	Catalog #2133; CAS 11032-79-4
PTX	Sigma-Aldrich	Catalog #P1675; CAS 124-87-8
TTX	Sigma-Aldrich	Catalog #554412; CAS 4368-28-9
Sulforhodamine 101	Invitrogen	Catalog #S359
Propofol	Sigma-Aldrich	Catalog #MKBK7900V; CAS 2078-54-8
Software and Algorithms		
ViewPoint (behavior analysis)	ViewPoint	http://www.viewpoint.fr
ImageJ (imaging analysis)	NIH	http://fiji.sc
MATLAB (Visual Stimulus)	MathWorks	http://www.mathworks.com/?requestedDomain=www.mathworks.com

Table 2. Zebrafish stains

Simple name	Full name	Type	Lab of Origin	ZFIN ID
Tg(UAS:GCaMP6s)	*Tg(5xUAS-hsp70l:GCaMP6s)nkUAShspzGCaMP6s13a*	Transgenic insertion	K. Kawakami Lab (Muto et al., 2017)	ZDB-ALT-170615-4
Ki(tph2:EGFP)	*Ki(tph2:EGFP)^{ion39d}*	Transgenic insertion	Jiu-Lin Du Lab (Li et al., 2015)	ZDB-ALT-170327-18
Ki(tph2:GAL4FF,cmlc2:EGFP)	*Ki(tph2:GAL4FF,myl7:EGFP)^{ion127d} (unpublished)*	Transgenic insertion	Jiu-Lin Du Lab	N/A
Tg(UAS:lyn-tdTomato)	*Tg(5xUAS-hsp:lyn-tdTomato)ion190d (unpublished)*	Transgenic insertion	Jiu-Lin Du Lab	N/A
Tg2(UAS:ChrimsonR-mKate2)	*Tg2(5×UAS-hsp:ChrimsonR-mKate2)ion236d (unpublished)*	Transgenic insertion	Jiu-Lin Du Lab	N/A

using an Olympus Fluoview FVMPE-RS multiphoton microscope equipped with a 25× water immersion objective (N.A., 1.05). The femtosecond laser was tuned to 920 nm for GCaMP6s imaging. Images were collected in Galvano-scanning mode controlled by Olympus elements software FV30S-SW. Dimming stimuli (2 s duration, 58 s interval) were applied simultaneously with a projector, with a red filter film added to avoid interference from white light. During in vivo calcium imaging, after imaging dimming-induced calcium activity for 10 min, propofol at final concentration of 30 μM was perfused for 30 min at a rate of 1.66 ml/min, followed by continuous perfusion of system water for elution until the end of imaging. During in vivo glutamate imaging, propofol was added to the dish by pipetting, with a total volume of 10 ml.

The obtained time series images were imported into ImageJ, and individual regions of interest (ROIs) were manually circled on the averaged images. Each ROI corresponds to a DRN$^{5\text{-HT}}$ neuron, and the average grayscale value in each ROI over time is noted as F. The F value was imported into MATLAB for further analysis, and the average F value of 10 min before the time zero of each ROI was taken as F_0. For the anesthesia process, the time point when the perfusion of propofol started or pipetting propofol was taken as the time zero; for the emergence process, the time point when the perfusion of elution started was taken as the time zero. The $\Delta F/F_0$ value of each ROI was calculated according to the formula $(F-F_0)/F_0$. Fish were imaged during the day only between 10 A.M. and 7 P.M.

Detection of induction and emergence time. Behavioral experiments were conducted on 7 dpf larvae between 10 A.M. and 7 P.M. Each larva was placed in a well of a 24-well plate, containing 1 ml system water per well. Larvae were acclimated to the plate under light for at least 20 min before experiments started. Propofol was added with 10 μl 0.1% DMSO (final concentration: 30 μM). The induction time of propofol was detected by two methods, according to Du et al. (2018): (1) mechanical stimulation, response to tail-fin pinch was tested by firmly applying pressure to the tail fin with nonserrated tissue forceps (Integra Miltex) every 10 s until it was inactive for 30 s, as described previously (Collymore et al., 2014; Du et al., 2018). Nonanesthetized larvae reacted to the pressure applied by twitching or attempting to swim away, whereas anesthetized larvae did not react. One author, well trained in pinching and blinded to the groups, performed the tail-fin pinches for all experimental larvae. The time between the application of propofol and the first inactivity was defined as the "induction time"; (2) spontaneous movements of the larvae were captured, and the distance and trajectory of the movements were automatically output by the ViewPoint tracking system in 10 s intervals. If larvae showed no movement in three consecutive cycles (30 s), the time of first inactivity was defined as the "induction time."

After 30 min of anesthesia, propofol was washed out, and the emergence time from GA was detected by two models: (1) the larvae were mechanically stimulated by tail-fin pinches with toothless forceps every 2 min until they responded for 6 min. The time between the elution of anesthetic and the first response to tail-fin pinches was defined as the "emergence time"; (2) the spontaneous movements of the larvae were captured, and the distance and trajectory of the movements were automatically output by the ViewPoint tracking system in 2 min intervals. If larvae showed movement in three consecutive cycles (6 min), the time of first movement was defined as the "emergence time."

Two-photon laser ablation. Two-photon laser ablation was performed using an Olympus Fluoview FVMPE-RS multiphoton microscope equipped with a 25× water immersion objective (N.A., 1.05). DRN$^{5\text{-HT}}$ neurons in *Ki(tph2:EGFP)* nacre larvae at 6 dpf were imaged before ablation and after ablation to confirm the effect of ablation, using a 940 nm laser for imaging and an 800 nm laser for ablation. The following parameters were used for local ablations: laser intensity 60%, laser duration 400 ms, laser interval 800 ms, and three iterations. All GFP-positive DRN$^{5\text{-HT}}$ neurons were ablated one by one in the order of from rostral to caudal, left to right. Ablations were considered successful when no GFP was observable and the cell membrane of the neuron was collapsed, as described in previous studies (Du et al., 2018; Oikonomou et al., 2019). In addition, the same number of cells surrounding the DRN$^{5\text{-HT}}$ neurons was randomly ablated as a mock ablation group using the same method. After ablation/mock ablation, larvae were carefully unmounted from the agarose gel and raised in the system water.

Two-photon ablation was conducted on 6 dpf larvae after behavioral experiments. After at least 12 h of recovery, paired behavioral experiments were performed on 7 dpf larvae. The same imaging parameters for each larva were used after the behavioral experiment at 7 dpf to observe the ablation efficacy (Fig. 2*A*). Larvae with ablation <70% were excluded from the statistical analysis.

Optogenetic activation. The ViewPoint tracking system was modified to include a custom array containing eight amber LEDs (590 nm, 5 W) mounted on the side wall 20 cm high and 10 cm away from the center of the 24-well plate to ensure uniform illumination. A power meter (Thorlabs, PM100D) was used to test the surface light intensity of the 24-well plate before each experiment (light intensity of ∼51–56 μw/mm^2). Field optogenetic activation was conducted by 3 s light exposure at 25 Hz followed by a 0.7 s break with a 2 min interval. Larvae were anesthetized with 30 μM propofol for 10 min, followed by elution with system water, and then placed in a 24-well plate with 1 ml system water in each well. The spontaneous movements of the larvae were captured, and the distance and trajectory of the movements were automatically output by the system in 2 min intervals. If larvae showed movement in three consecutive cycles (6 min), the time of first movement was defined as the "emergence time."

To detect if optogenetic activation by 590 nm LED light influences the larval spontaneous movements, locomotion was monitored by the ViewPoint tracking system at 7 dpf. Before recording, each larva was put in an individual well of a 24-well plate under light background for 15 min for adaptation. Spontaneous locomotion activity of each larva was recorded and tracked in real time for 1 h, and the swimming distance was calculated per 10 min automatically.

In vivo whole-cell recording. In vivo electrophysiological recording experiments were performed in 5–8 dpf larvae. Larvae were paralyzed with 0.1% α-bungarotoxin and then transferred to a glass-bottomed Petri dish and embedded with 1.5% low-melting point agarose gel dorsal side up. After gel solidification, larvae were submerged in extracellular solution (134 mM NaCl, 2.9 mM KCl, 2.1 mM $CaCl_2$, 1.2 mM $MgCl_2$, 10 mM HEPES, 10 mM glucose; 290 mOsmol/L), pH 7.8. The gel over the ventricles between the cerebellum and the hindbrain was peeled off with a glass micropipette, and a transverse incision was made in the skin, ∼30 μm in diameter. Glass micropipettes (20–25 MΩ in resistance, 1–2 μm tip diameter) were made from borosilicate glass capillaries (BF 100-58-10, Sutter Instruments) using a Flaming/Brown P97 micropipette puller (Sutter Instruments). Intracellular solution (110 mM K-gluconate, 6 mM NaCl, 2 mM $MgCl_2$, 2 mM $CaCl_2$, 10 mM HEPES, 10 mM EGTA;

270 mOsmol/L), pH 7.4, was perfused into the micropipette, and continuous positive pressure (10–30 cmH_2O) was applied. A micromanipulator (MP-225, Sutter Instruments) was used to control the micropipette into the incision and close to the target $DRN^{5\text{-}HT}$ neuron. The previously applied positive pressure was removed, and a negative pressure was applied to form a Giga-seal (resistance >1 GΩ). The holding potential was then adjusted to −60 mV, and after waiting for the seal to stabilize, a strong and brief negative pressure was applied to break the cell membrane at the tip seal to achieve in vivo whole-cell recording. The signal was recorded using a MultiClamp 700B amplifier (Axon Instruments), filtered with a 2 kHz low-pass filter, and acquired at 10 kHz. The data were imported into a computer using a Digidata 1440A (Axon Instruments) and then acquired, stored, and analyzed using Clampex 10.2 (Molecular Devices). Data were excluded if the series resistance changed by >20% or if the resting potential of the cell membrane was above −40 mV.

Local puffing and bath application of drugs. Propofol was injected into the micropipette tip using a micro filler, and the micropipette was moved 50 μm from the $DRN^{5\text{-}HT}$ neuron using a micromanipulator under high magnification (60×). Propofol was applied topically to the vicinity of the recorded neuron using a pressure pulse generated by the picrospritzer (1–2 μm tip diameter, 5–10 psi pulse intensity, 300–500 ms duration, 1 s interval, 30–60 s total administration time). Sulforhodamine 101 was locally puffed in the central area of the DRN by similar parameters for the picrospritzer. For bath application, the concentrations of tetrodotoxin (TTX) and picrotoxin (PTX) were 2 and 100 μM, respectively.

Statistical analysis. The Kolmogorov–Smirnov test was used to test whether the data were normally distributed. For the comparison of two groups, if the data were normally distributed and the variances were χ^2, the two-tailed paired or unpaired Student's t test was used to test the significance of the differences between paired and unpaired data, respectively; when the variances were not χ^2, Welch's t test was used. If the data were not normally distributed, the Wilcoxon sign-rank test or Wilcoxon rank-sum test was used to test the significance of the difference between two paired or unpaired data groups, respectively. For multiple comparisons, the one-way ANOVA followed by Tukey's multiple-comparison test was used to analyze the significance of data differences when the data were normally distributed, and the Kruskal–Wallis test was used to compare the significance of data differences when the data were not normally distributed. A $p < 0.05$ was considered statistically significant. All statistical results are shown as mean ± SEM.

Results

$DRN^{5\text{-}HT}$ neuronal activity is suppressed by propofol anesthesia

In vertebrates, 5-HT is synthesized in multiple brain regions, including the pineal gland, preoptic area, posterior tuberculum, hypothalamus, midbrain/pons, and medulla oblongata. The raphe nuclei span the midbrain/pons boundary and medulla (Lillesaar et al., 2009). In zebrafish larvae, the raphe nuclei are subdivided into superior raphe (also termed as DRN) and inferior raphe. Tryptophan hydroxylase (tph) is the rate-limiting enzyme in 5-HT synthesis, and only tph2 is expressed in the raphe among the three tph paralogs in the zebrafish genome (Teraoka et al., 2004). We generated a zebrafish tph2 knock-in mutant line *Ki(tph2:GAL4FF,cmlc2:EGFP)* using genome editing.

To examine the calcium activity of $DRN^{5\text{-}HT}$ neurons during propofol anesthesia, we crossed *Ki(tph2:GAL4FF,cmlc2:EGFP)* with a transgenic fish line *Tg(UAS:GCaMP6s)* (Fig. 1*A*) and recorded calcium imaging of $DRN^{5\text{-}HT}$ neurons at cellular resolution using two-photon microscopy. Due to the relatively low spontaneous calcium activity of $DRN^{5\text{-}HT}$ neurons, we tested three types of visual stimuli (dimming, flash, and looming; Yao et al., 2016) to increase calcium events, among which dimming was the most effective and stable ($n = 210$ neurons from three larvae; Fig. 1*B*,*C*). Therefore, calcium imaging was recorded under dimming stimulation at 58 s intervals (Fig. 1*D*,*F*), which did not influence the membrane potential of $DRN^{5\text{-}HT}$ neurons, as detected by in vivo whole-cell electrophysiology (Fig. 1*E*). Calcium activity of $DRN^{5\text{-}HT}$ neurons gradually decreased after the onset of 30 μM propofol perfusion (Fig. 1*F*,*H*,*I*; pre-propofol vs pro, 0 vs −0.390 ± 0.007; $p < 0.001$; paired t test; $n = 221$ $DRN^{5\text{-}HT}$ neurons from three larvae) and did not recover until perfusion stopped (Fig. 1*G*,*J*,*K*; propofol vs post pro, 0 vs 0.305 ± 0.035; $p < 0.001$). The EC_{50} of propofol to exert hypnotic effect on larval zebrafish is 1.1, and 30 μM reversibly inhibited 100% of the photomotor response, as tested in our previous work (Yang et al., 2018, 2019). The slow recovery of neural activity is attributed to the slow perfusion speed (1.66 ml/min) to ensure imaging stability and potential quenching of GCaMP6s fluorescence signal over long imaging periods (Extended Data Fig. 1-1). These results imply that $DRN^{5\text{-}HT}$ neurons are influenced by propofol-induced GA.

Ablation of $DRN^{5\text{-}HT}$ neurons retards emergence from propofol anesthesia

To further investigate the role of $DRN^{5\text{-}HT}$ neurons in propofol GA, we locally ablated $DRN^{5\text{-}HT}$ neurons using a two-photon laser in *Ki(tph2:EGFP)* larvae at 6 dpf. The experimental diagram is depicted in Figure 2*A*. Induction time was detected by loss of response to mechanical stimuli and loss of spontaneous movement, and emergence time was detected by the recovery of response to mechanical stimuli and spontaneous movement. After behavioral assays, each larva was reimaged to confirm the efficacy of ablation, indicated by a significant decrease in EGFP fluorescence signal (Fig. 2*B*).

To identify the appropriate concentration of propofol for behavioral experiments, 6 dpf larvae were incubated with different concentrations (0, 3, 6, 9, 15, 30, and 100 μM) and immediately measured for touch responses to tail-fin pinches to evaluate induction time. Larvae exhibited a dose-dependent loss-of-response rate to tail-fin pinch, showing no response ∼4 min after treatment with propofol at concentrations ≥30 μM, while 15 μM and below failed to induce a 100% loss-of-response rate for up to 10 min (Fig. 2*C*). Considering tens of micromolar propofol in human blood during anesthesia and the induction time (only a few minutes; Brown et al., 2011), we initially chose 30 μM for behavioral experiments.

We found that ablation of $DRN^{5\text{-}HT}$ neurons had little effect on the induction time of propofol anesthesia (Fig. 2*D*,*E*; mechanical stimulation, control group, 247.1 ± 12.1 min; mock ablation, 250.6 ± 10.7 min; DRN ablation, 249.4 ± 11.2 min; $p > 0.05$; spontaneous movement, control group, 37.4 ± 3.4 s; mock ablation, 34.1 ± 3.6 s; DRN ablation, 36.4 ± 3.2 s; $p > 0.05$; one-way ANONA) but altered the emergence time (Fig. 2*F*,*G*). Compared with the control group, emergence time was significantly prolonged in the DRN ablation group, with no difference between control and mock ablation groups, as detected by mechanical stimulation (Fig. 2*F*; $F = 5.91$; control vs DRN ablation; 11.5 ± 1.0 min vs 16.5 ± 1.7 min; $p = 0.019$). Similar results were observed for the emergence time based on spontaneous movement recovery (Fig. 2*G*; $F = 5.70$; control vs DRN ablation; 81.0 ± 3.7 min vs 95.4 ± 4.2 min; $p = 0.036$).

Considering the high concentration of propofol might mask induction dynamics around the EC_{50} (Franks, 2008), we tested induction time under 1 and 3 μM propofol (Fig. 2*H*–*K*). The loss of response rate to mechanical stimulation 30 min after adding 3 μM propofol was similar among the three groups (Fig. 2*H*).

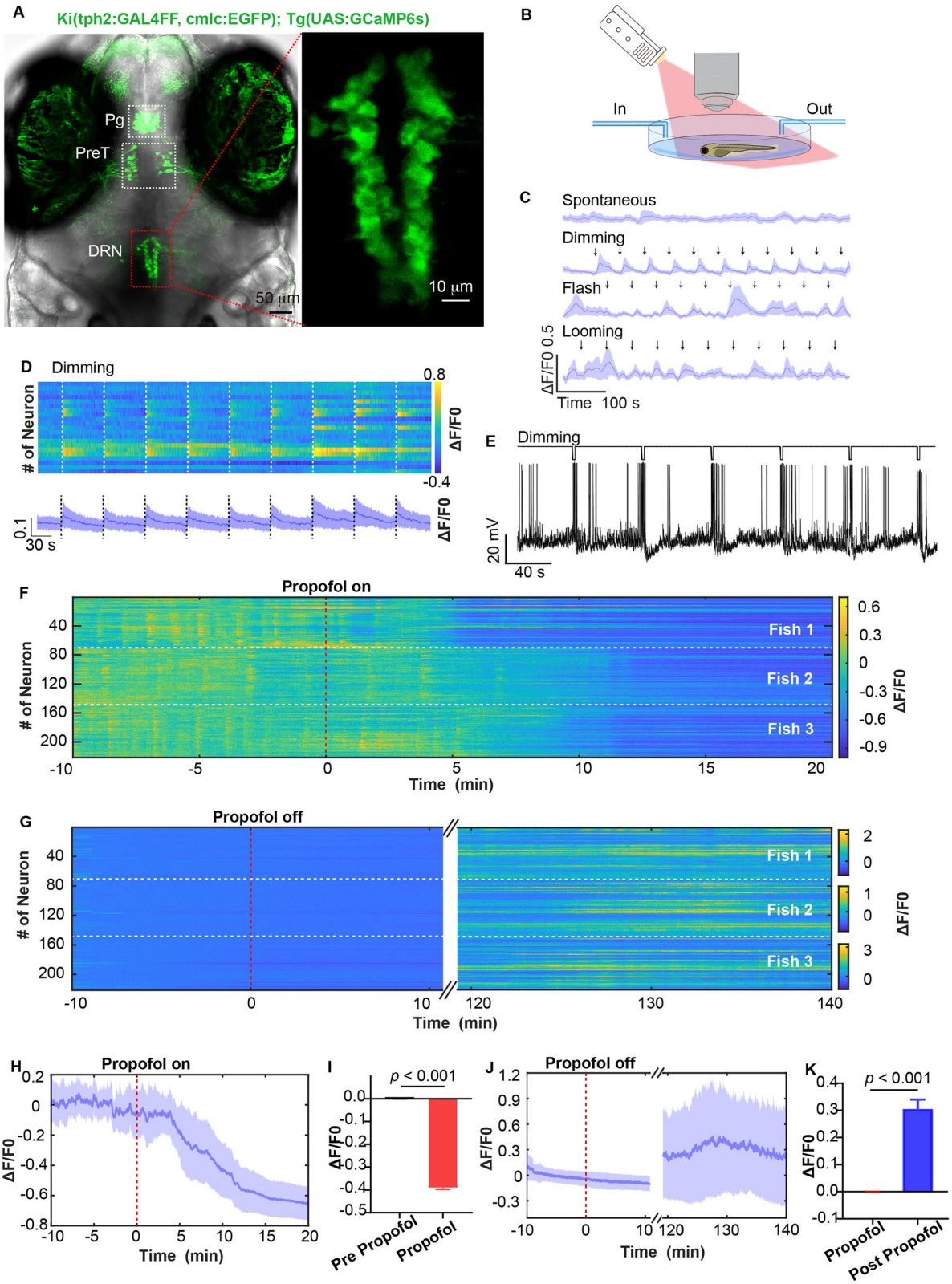

Figure 1. Calcium activity of DRN$^{5\text{-HT}}$ neurons were suppressed by propofol. ***A***, The tph2 knock-in mutant line *Ki(tph2:GAL4FF,cmlc2:EGFP);Tg(UAS:GCaMP6s)* marks 5-HT neuron at pineal gland (Pg), pretectum (PreT), and DRN. ***B***, Propofol was perfused and eluted during in vivo calcium imaging at single cellular resolution, accompanied by visual stimuli by a projector. ***C***, Spontaneous calcium activity of DRN$^{5\text{-HT}}$ and calcium activity responded to dimming, flash and looming stimuli. Data represent mean ± SEM. $n = 3$ larvae. ***D***, Representative calcium activity stimulated by dimming at 58 s interval (top) and the mean trace (bottom) from a layer of DRN$^{5\text{-HT}}$. The dash line indicates dimming stimulation. Data represent mean ± SEM. ***E***, In vivo whole-cell electrophysiology showed not that dimming stimuli did not influence the membrane potential of DRN$^{5\text{-HT}}$. ***F***,***G***, Heatmaps of calcium activity during perfusion and elution of propofol from 221 DRN$^{5\text{-HT}}$ neuron of three larvae. The slow recovery of neural activity is attributed to the slow perfusion speed (1.66 ml/min) to ensure imaging stability and potential quenching of GCaMP6s fluorescence signal over long imaging periods (Extended Data Fig. 1-1). ***H***,***I***, Calcium events were significantly inhibited by 30 μM propofol perfusion. ***H***, mean ± SEM, indicated by the full line and shaded area. ***I***, Pre-propofol versus propofol; 0 versus −0.390 ± 0.007; $p < 0.001$; paired t test. ***J***,***K***, Calcium activity recovered after propofol was eluted. ***J***, Mean ± SEM, indicated by the full line and shaded area. ***K***, Propofol versus post-propofol, 0 versus 0.305 ± 0.035; $p < 0.001$; paired t test.

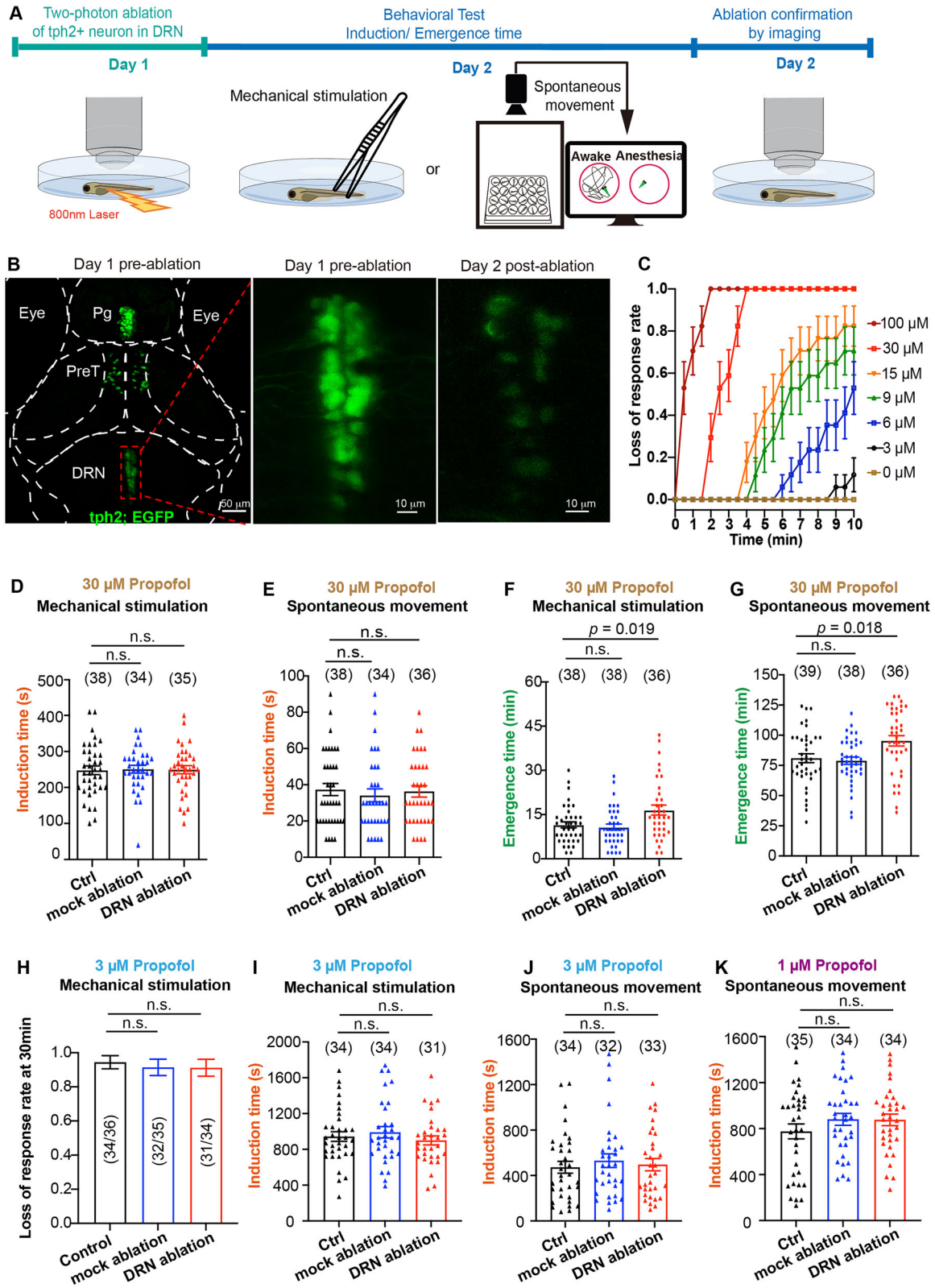

Figure 2. Two-photon laser ablation of DRN$^{5\text{-HT}}$ neurons retarded emergence from propofol anesthesia. ***A***, Behavioral experiments diagram. ***B***, The representative images of two-photon laser ablation on DRN$^{5\text{-HT}}$ neurons. ***C***, Dose response curve of propofol on the loss-of-response to tail-fin pinch. $N = 21$ larvae/concentration. ***D***,***E***, Specific ablation of DRN$^{5\text{-HT}}$ had little effect on the induction time of 30 μM propofol anesthesia detected by mechanical stimulation (***D***, control group, 247.1 ± 12.1 min; mock ablation, 250.6 ± 10.7 min; DRN ablation, 249.4 ± 11.2 min; $p > 0.05$; one-way ANOVA) and loss of spontaneous movement (***E***, control group, 37.4 ± 3.4 min; mock ablation, 34.1 ± 3.6 min; DRN ablation, 36.4 ± 3.2 min; $p > 0.05$; one-way ANOVA). ***F***,***G***, Specific ablation of DRN$^{5\text{-HT}}$ significantly prolonged emergence time from 30 μM propofol, detected by both recovery to mechanical stimulation (***F***, $F = 5.91$, control vs DRN ablation; 11.5 ± 1.0 min vs 16.5 ± 1.7 min; $p = 0.019$; one-way ANOVA) and the recovery time of spontaneous movement (***G***, $F = 5.70$; control vs DRN ablation; 81.0 ± 3.7 min vs 95.4 ± 4.2 min; $p = 0.036$; one-way ANOVA). ***H–J***, Specific ablation of DRN$^{5\text{-HT}}$ had little effect on the induction time of 3 μM propofol anesthesia detected by mechanical stimulation (***H***, loss of response rate at 30 min; ***I***, induction time, control group, 943.2 ± 53.8 s; mock ablation, 990.9 ± 63.6 s; DRN ablation, 900.0 ± 50.6 s; $p > 0.05$; one-way ANONA) and loss of spontaneous

Two-photon laser ablation of DRN$^{5\text{-HT}}$ neurons did not influence induction time at 3 μM, as tested by loss of response rate to mechanical stimulation (Fig. 2*I*; control group, 943.2 ± 53.8 s; mock ablation, 990.9 ± 63.6 s; DRN ablation, 900.0 ± 50.6 s; $p > 0.05$; one-way ANONA) and loss of spontaneous movement (Fig. 2*J*; control group. 472.6 ± 52.4 s; mock ablation, 495.3 ± 54.1 s; DRN ablation, 530.3 ± 59.9 s; $p > 0.05$; one-way ANONA). A 1 μM propofol did not induce a loss of response to mechanical stimulation even at 1 h after addition in all groups (data not shown). Two-photon laser ablation of DRN$^{5\text{-HT}}$ neurons did not influence induction time at 1 μM, as tested by loss of spontaneous movement (Fig. 2*K*; control group, 776.0 ± 64.5 s; mock ablation, 880.6 ± 51.8 s; DRN ablation, 876.2 ± 50.1 s; $p > 0.05$; one-way ANONA).

These results suggest that DRN$^{5\text{-HT}}$ neurons play an emergence-promoting role in propofol anesthesia, while their role in the induction process was not observed at 1, 3, and 30 μM.

Optogenetic activation of DRN$^{5\text{-HT}}$ neurons promotes emergence from propofol anesthesia

To determine whether activation of DRN$^{5\text{-HT}}$ neurons is sufficient to drive emergence, we utilized *Ki(tph2:GAL4FF,cmlc2:EGFP); Tg(UAS:ChrimsonR-mKate)* transgenic lines in which ChrimsonR was expressed in DRN$^{5\text{-HT}}$ neurons (Fig. 3*A*). Optical activation by LED (0.3 s light exposure at 25 Hz followed by a 0.7 s break) was performed repeatedly by 30 s trials with a 2 min interval (Fig. 3*B*). In vivo cell-attached recording showed that 5-HT neurons expressing ChrimsonR fired in response to 590 nm light pulses at 25 Hz (Fig. 3*C*). We used a modified video-tracking system to monitor spontaneous movements (Fig. 3*D*) and found no difference in the distance moved under optogenetic stimulation between the tph2:ChrimsonR− and tph2:ChrimsonR+ groups (349.8 ± 21.7 mm vs 353.0 ± 15.8 mm; $p > 0.05$; Fig. 3*E–G*). After washing out propofol (Fig. 3*H*), emergence time was evaluated by recovery of spontaneous movement (Fig. 3*I*) and response to tail-fin pinch (Fig. 3*J*) under 590 nm LED lights. Optogenetic activation of tph2+ neurons significantly promoted emergence from propofol anesthesia (Fig. 3*I*; tph2:ChrimsonR−, 80.2 ± 3.5 min; tph2:ChrimsonR+, 65.3 ± 3.3 min; $p = 0.003$; Fig. 3*J*; tph2:ChrimsonR−, 15.5 ± 1.2 min; tph2:ChrimsonR+, 10.3 ± 1.0 min; $p = 0.001$; unpaired Student's *t* test).

To confirm that optical field stimulation of tph2+ neurons specifically activates DRN$^{5\text{-HT}}$ neurons, rather than those in the pineal and pretectal regions, we ablated tph2+ neurons in these regions using *Ki(tph2:EGFP)* fish lines and tested emergence time by recovery of response to mechanical stimulation and spontaneous movement (Fig. 4*A*). Ablation of tph2+ neurons in the pineal and pretectal regions (Fig. 4*B*) did not change the locomotor activity (Fig. 4*C,D*) or emergence time (Fig. 4*E,F*), indicating that the shortened emergence time observed with optical field activation is mainly due to optogenetic activation of DRN$^{5\text{-HT}}$ neurons.

Propofol decreases the excitability of DRN$^{5\text{-HT}}$ by inhibiting presynaptic glutamate excitatory inputs and enhancing inhibitory GABA$_A$ receptor activity

To examine how propofol acts on DRN$^{5\text{-HT}}$, we performed whole-cell current–clamp recording of DRN$^{5\text{-HT}}$ on *Ki(tph2:GAL4FF,cmlc:EGFP);Tg(UAS:lyn-tomato)* larvae. Lyn is a member of the Src-family of kinases and is expressed in a wide variety of cell types, anchored to cellular membranes (Brian and Freedman, 2021). The boundary of DRN$^{5\text{-HT}}$ was visualized clearly using the *tph2:GAL4;UAS:lyn-tdTomato* fish line, facilitating whole-cell recording (Fig. 5*A*). Local puffing of propofol to DRN$^{5\text{-HT}}$ neurons (Fig. 5*B*) almost completely suppressed spontaneous spike firing (Fig. 5*C,D*; pre vs post, 0.10 ± 0.02 Hz vs 0.00 ± 0.00 Hz; $p = 0.001$; pre vs recovery, 0.10 ± 0.02 Hz vs 0.05 ± 0.02 Hz; $p > 0.05$) and hyperpolarized DRN$^{5\text{-HT}}$ neurons (Fig. 5*C,E*; pre vs post, −55.1 ± 1.5 mV vs −62.0 ± 3.1 mV; $p = 0.019$). Spiking activity recovered ∼20 min after puffing. Furthermore, spike firing evoked by current injection was significantly suppressed by propofol (Fig. 5*F,G*; $p = 0.012$ for pre- vs post-propofol) and caused a decrease in membrane input resistance of DRN$^{5\text{-HT}}$ neurons (Fig. 5*H*; pre vs post, 2.0 ± 0.3 GΩ vs 1.6 ± 0.3 GΩ; $p = 0.019$). Taken together, these results indicate that propofol reduces the excitability of DRN$^{5\text{-HT}}$ neurons.

Given that propofol is an agonist of GABA$_A$ receptors (Franks, 2008), the suppression of DRN$^{5\text{-HT}}$ neurons' excitability can be attributed to the blockade of presynaptic excitatory inputs and/or enhancement of tonic inhibition of these neurons. To examine these possibilities, we performed whole-cell voltage–clamp recording on DRN$^{5\text{-HT}}$ neurons. Local puffing of propofol largely abolished excitatory postsynaptic currents (EPSCs; Fig. 6*A,B*; pre vs post: 4.95 ± 1.36 Hz vs 0.40 ± 0.26 Hz; $p = 0.008$), implying that propofol may block presynaptic excitatory inputs to DRN$^{5\text{-HT}}$ neurons. Moreover, application of propofol induced an outward current (Fig. 6*A,C*; 4.5 ± 1.6 pA).

To further confirm the effect of propofol on presynaptic excitatory inputs of DRN$^{5\text{-HT}}$ neurons, we expressed an improved version of iGlusnFR3 (Aggarwal et al., 2023) on DRN$^{5\text{-HT}}$ neurons, which directly indicates the presynaptic input to DRN$^{5\text{-HT}}$ neurons. Propofol was gently added (60 μl 5 mM) into 10 ml dish and eluted by perfusion (1.66 ml/min) 30 min after addition. A 30 μM propofol completely abolished the presynaptic glutamate events of DRN$^{5\text{-HT}}$ neurons induced by dimming stimulation (Fig. 6*D–F*; pre-propofol vs propofol; 0 vs −0.393 ± 0.018; $p < 0.001$; paired *t* test; $n = 259$ DRN$^{5\text{-HT}}$ neurons from three larvae). iGlusnFR3 signal gradually recovered when propofol was eluted by perfusion (Fig. 6*G,H*; propofol vs post pro; 0 vs 0.589 ± 0.023; $p < 0.001$). Together with the observation that propofol inhibited the EPSC frequency of DRN$^{5\text{-HT}}$, our data indicate that propofol blocks the presynaptic excitatory glutamate inputs of DRN$^{5\text{-HT}}$ neurons.

To further examine the effect of propofol on DRN$^{5\text{-HT}}$ neurons per se, we abolished synaptic transmission by replacing Ca^{2+} with 4 mM Co^{2+} in the extracellular solution to block Ca^{2+}-dependent transmitter release and adding 1 mM TTX, an antagonist of voltage-gated sodium channels, to suppress the generation of action potentials. This is a commonly used pharmacological method to isolate neurons and study the intracellular effect of an administered agent (Du et al., 2018). Under these conditions, local puffing of propofol caused significant hyperpolarization of DRN$^{5\text{-HT}}$ neurons, indicating that propofol suppressed the excitability of DRN$^{5\text{-HT}}$ neurons per se. Moreover, this hyperpolarization was completely abolished by bath application of 100 mM

←

movement (***J***, control group, 472.6 ± 52.4 s; mock ablation, 495.3 ± 54.1 s; DRN ablation, 530.3 ± 59.9 s; $p > 0.05$; one-way ANOVA). ***K***, Specific ablation of DRN$^{5\text{-HT}}$ had little effect on the induction time of 1 μM propofol anesthesia detected by loss of spontaneous movement (control group, 776.0 ± 64.5 s; mock ablation, 880.6 ± 51.8 s; DRN ablation, 876.2 ± 50.1 s; $p > 0.05$; one-way ANOVA). The sample size for each group is indicated in parentheses. In **H**, the values in parentheses are the ratio of the number of larvae that lost response to the total sample size.

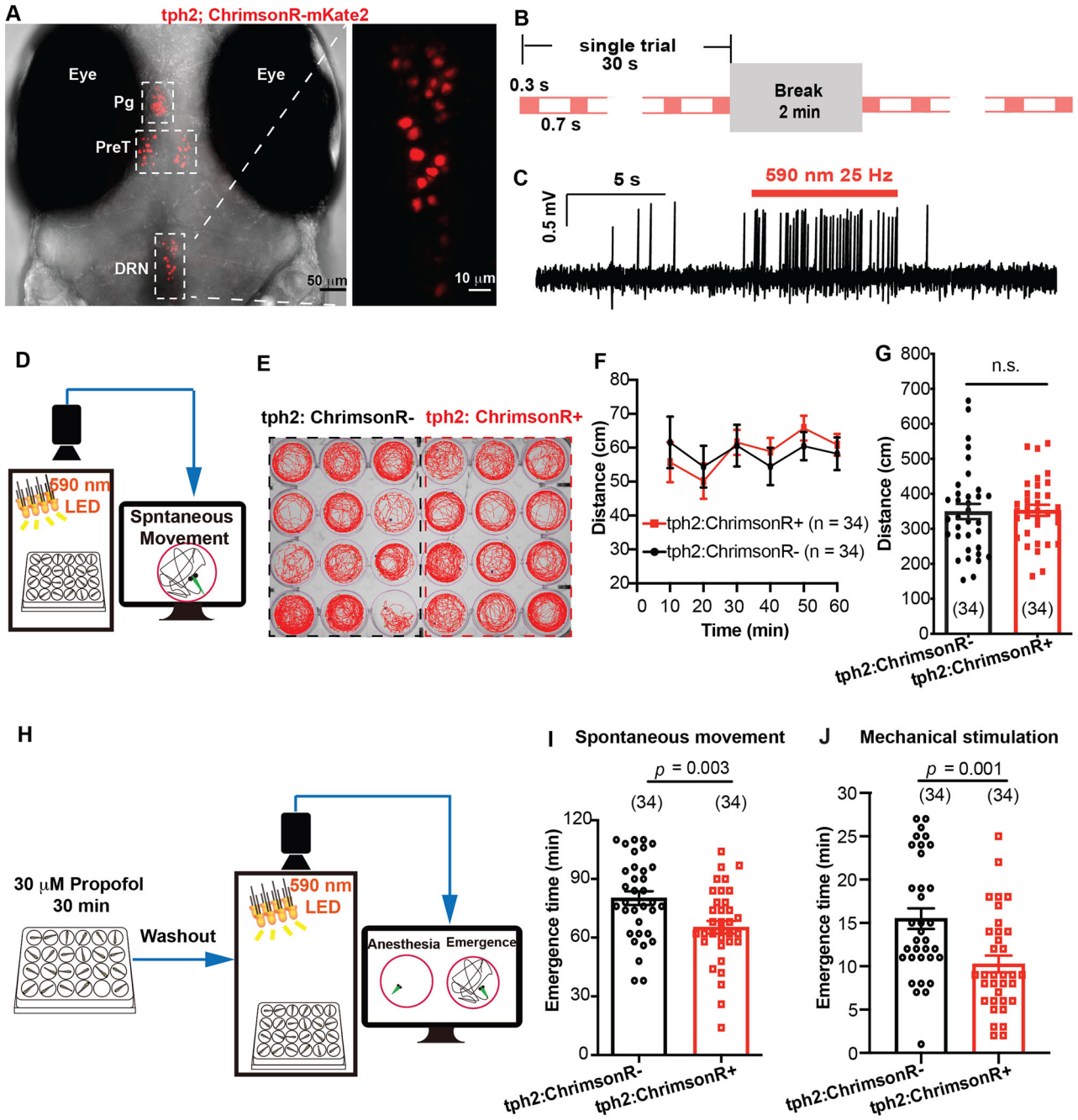

Figure 3. Optogenetic activation of tph2+ neurons promoted emergence from propofol anesthesia. ***A***, The expression of *Ki(tph2: GAL4FF,cmlc2:EGFP);Tg(UAS: ChrimsonR-mKate2)* mutant line. Pg, pineal gland; PreT, pretectum; DRN, dorsal raphe nucleus. ***B***, Optogenetic stimulation paradigm during the whole process of emergence. ***C***, Confirmation of ChrimsonR activation by in vivo cell-attached recording. ***D***, The diagram of behavior experiment detecting the influence of field optogenetic activation on locomotor activity. ***E***, The spontaneous movement trajectory under optogenetic stimulation during 10 min. ***F***,***G***, Distance moved under optogenetic stimulation during 1 h and the statistical analysis (tph2, ChrimsonR−, vs tph2, ChrimsonR+; 349.8 ± 21.7 mm vs 353.0 ± 15.8 mm; $p > 0.05$; unpaired Student's *t* test). ***H***, The diagram of behavioral experiment detecting the influence of field optogenetic activation on the emergence time from propofol. ***I***,***J***, Optogenetic stimulation significantly promoted the emergence from propofol anesthesia detected by recovery of spontaneous movement and recovery to mechanical stimulation (spontaneous movement, tph2, ChrimsonR−, vs tph2, ChrimsonR+; 80.2 ± 3.5 min vs 65.3 ± 3.3 min; $p = 0.003$; mechanical stimulation, tph2, ChrimsonR−, 15.5 ± 1.2 min; tph2, ChrimsonR+, 10.3 ± 1.0 min; $p = 0.001$; unpaired Student's *t* test). The sample size for each group is indicated in parentheses.

PTX, an antagonist of $GABA_A$ receptors (Fig. 6*I*,*J*; without PTX vs with PTX, −5.2 ± 1.3 mV vs 0.2 ± 0.2 mV; $n = 5$; $p = 0.013$; paired Student's *t* test). Taken together, these results indicate that propofol suppresses the activity of $DRN^{5\text{-}HT}$ neurons by both inhibiting the activity of $DRN^{5\text{-}HT}$ per se through $GABA_A$ receptors and blocking presynaptic excitatory glutamate inputs.

To fully elucidate the role of $GABA_A$ receptors in $DRN^{5\text{-}HT}$ neurons in the induction and emergence time of propofol, PTX was locally puffed to the DRN area before adding propofol. A red fluorescent dye, sulforhodamine 101, with a molecular weight close to that of propofol, was puffed together to precisely control the position and volume of puffing. Induction and emergence time were evaluated by tail-fin pinch. As shown in Figure 6*K*–*N*, inhibiting $GABA_A$ receptors in the DRN by local puffing PTX had no influence on induction time but significantly shortened the emergence time from propofol anesthesia (Fig. 6*N*;

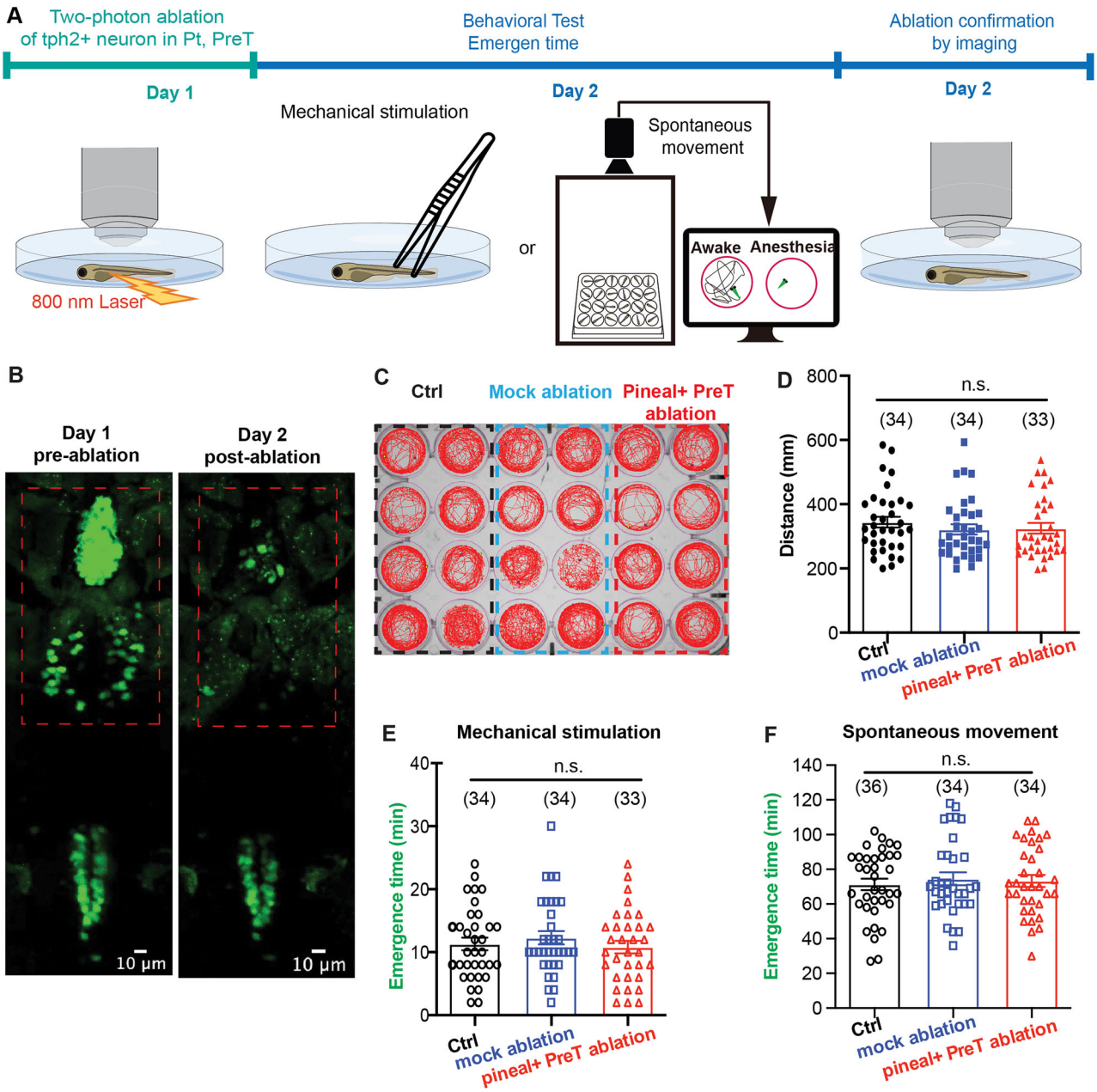

Figure 4. Two-photon laser ablations of tph2+ neurons in pineal and pretectum did not influence the emergence from propofol. ***A***, Behavioral experiments diagram. ***B***, The representative images of two-photon laser ablation on pineal and pretectum. ***C***, The spontaneous movement trajectory of the control group, mock ablation group, and pineal + pretectum ablation group during 10 min. ***D***, Distance moved during 1 h and the statistical analysis (control vs mock ablation vs pineal + preT ablation; 349.8 ± 18.0 mm vs 330.1 ± 17.5 mm vs 336.5 ± 17.7 mm; $p > 0.05$; unpaired Student's *t* test). ***E,F***, Two-photon laser ablations of pineal and pretectum did not influence the emergence time from propofol anesthesia, detected by both recovery to mechanical stimulation (***E***, control, 11.3 ± 1.0 min; mock ablation, 12.3 ± 1.0 min; pineal + PreT ablation, 10.8 ± 1.0 min) and the recovery time of spontaneous movement (***F***, control, 71.3 ± 3.3 min; mock ablation, 74.5 ± 3.8 min; pineal + PreT ablation, 73.3 ± 3.5 min). $p > 0.05$; one-way ANOVA.

dye vs dye + PTX; 13.8 ± 1.2 min vs 10.3 ± 1.0 min; $p = 0.036$). Since most neurons in the DRN of zebrafish are tph2-positive 5-HT neurons (Oikonomou et al., 2019), these data indicate that $GABA_A$ receptors on $DRN^{5\text{-HT}}$ neurons are involved in the hypnotic effect of propofol.

In addition to $GABA_A$ receptors, propofol exerts additional attenuation on glutamatergic synaptic signaling mediated by both AMPA and NMDA receptors (Luppi et al., 2023), possibly through allosteric modulation of channel gating rather than blocking the open channel (Orser et al., 1995). To examine if propofol inhibited the excitability of $DRN^{5\text{-HT}}$ neurons per se through glutamatergic receptors, we performed in vivo whole-cell recording while blocking glutamatergic receptors by adding 50 μM CNQX and 100 μM APV in the extracellular solution, which are antagonists of AMPA and NMDA receptors, respectively. After blocking glutamatergic receptors, local puffing of propofol caused significant hyperpolarization of $DRN^{5\text{-HT}}$ neurons (mean ± SEM, −5.7 ± 0.9 mV; $n = 5$ neurons from different larvae; Fig. 6*O,P*), suggesting that the suppression of $DRN^{5\text{-HT}}$ neurons by propofol is independent of glutamatergic receptors.

Discussion

Emergence from GA proceeds more slowly and variably than anesthesia induction, typically considered a passive process after

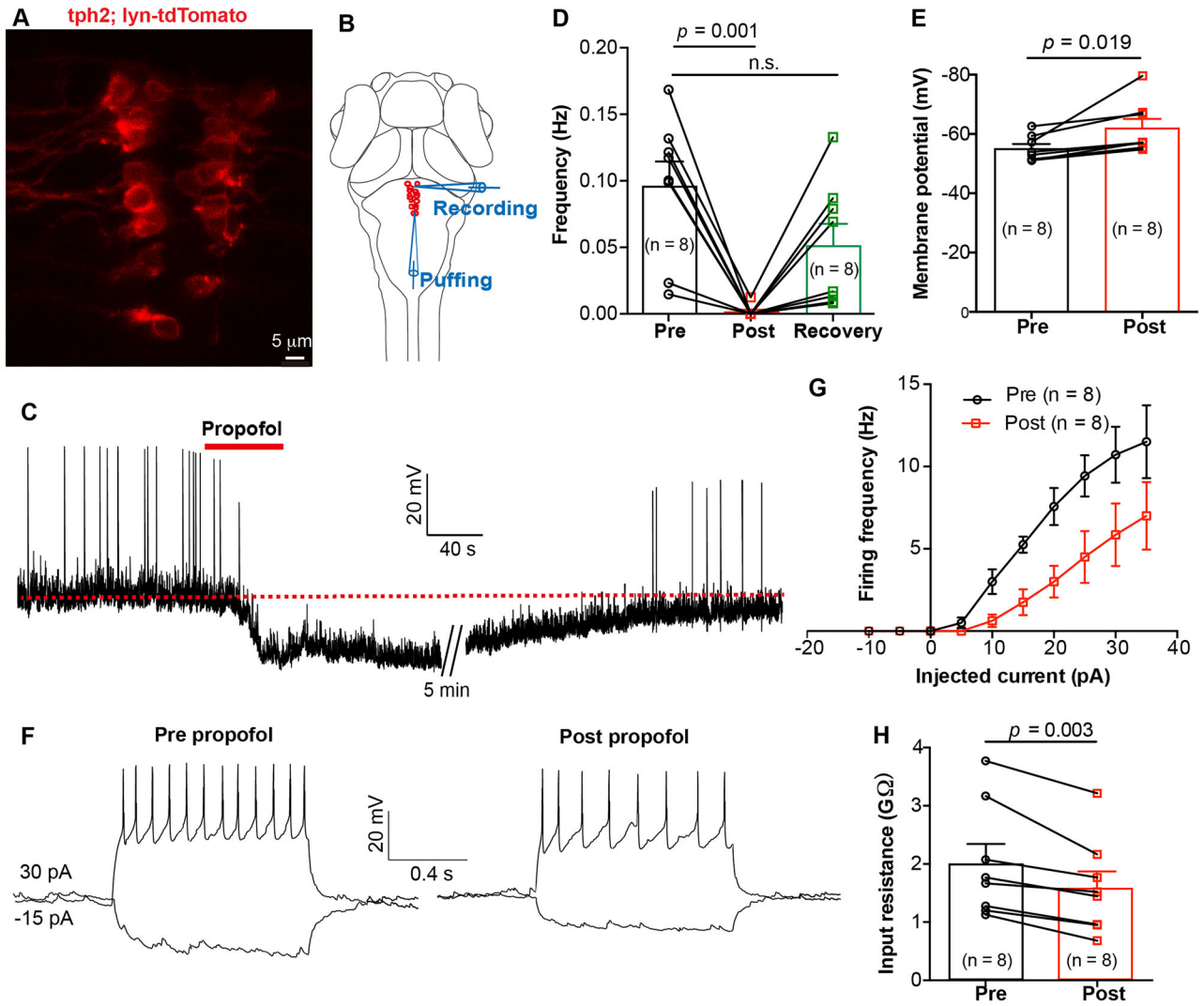

Figure 5. In vivo whole-cell recording revealed that propofol decreased the excitability of DRN$^{5\text{-HT}}$. ***A***, The expression of *Ki(tph2:GAL4FF,cmlc2:EGFP);Tg(UAS: lyn-tdTomato)* mutant line at dorsal raphe. ***B***, Schematic diagram showing whole-cell recording of DRN$^{5\text{-HT}}$ neurons and simultaneous local puffing of propofol onto DRN$^{5\text{-HT}}$. ***C***, Spontaneous spike firing of DRN$^{5\text{-HT}}$ neuron before and after puffing of propofol. The red dashed line indicates the mean resting membrane potential before propofol treatment. ***D***,***E***, Summary of data showing the effect of propofol treatment on the spontaneous spike frequency (***D***, pre vs post, 0.10 ± 0.02 Hz vs 0.00 ± 0.00 Hz; $p = 0.001$; pre vs recovery, 0.10 ± 0.02 Hz vs 0.05 ± 0.02 Hz; $p > 0.05$; paired Student's *t* test) and resting membrane potential (***E***, pre vs post, -55.1 ± 1.5 mV vs -62.0 ± 3.1 mV; $p = 0.019$; paired Student's *t* test) of DRN$^{5\text{-HT}}$ neurons. Pre, before puffing; post, immediately after puffing; recovery, 10 min after puffing. ***F***, Representative traces showing voltage responses of DRN$^{5\text{-HT}}$ evoked by current injections before (left) and immediately after (right) puffing of propofol. ***G***, Summary of data showing the effect of propofol on current injection-evoked spike firing of DRN$^{5\text{-HT}}$ neurons. $p = 0.01$, Kolmogorov–Smirnov test. ***H***, Summary of data showing the effect of propofol on the membrane resistance of DRN$^{5\text{-HT}}$ neurons. Pre versus post, 2.0 ± 0.3 versus 1.6 ± 0.3 GΩ; $p = 0.019$; paired Student's *t* test. Numbers of cells examined are in parentheses.

the discontinuation of anesthetic agents. Patients are monitored for the recovery of physiological and behavioral signs of consciousness, which can sometimes be accompanied by medical complications, especially in the elderly or vulnerable surgical patients (Brown et al., 2010). Currently, no medications are available to actively reverse GA or speed up emergence in patients (Cylinder et al., 2024). Therefore, understanding the neural systems involved in emergence is fundamental to optimizing anesthetic safety and enhancing our knowledge of anesthetic action.

Studying the mechanism of GA is challenging due to the wide range of effects on the nervous system, which is inherently complex with extensive connections. As such, a simple and conserved animal model is required for in vivo studies. Our previous work introduced zebrafish as a vertebrate animal model advantageous for pharmacologic studies of intravenous sedative–hypnotics (Yang et al., 2018, 2019). Zebrafish larvae rapidly equilibrate with aqueous drugs through transdermal and respiratory pathways, allowing for high-throughput drug effect studies at steady state and avoiding pharmacodynamic variation seen with complex drug pharmacokinetics in mice (Yang et al., 2018). Additionally, their transparency, genetic accessibility, and extensive anatomical and neurochemical homology to mammals enable in vivo calcium imaging and whole-cell recording at single-cell resolution, uncovering conserved neuromodulatory circuits with superior spatial and temporal precision (Oikonomou et al., 2019). The conserved nature of the 5-HT system and anesthesia behavior suggests that insights gained from zebrafish could be translatable to mammals.

Here we confirmed the role of DRN$^{5\text{-HT}}$ neurons in facilitating the emergence from propofol anesthesia but not in anesthesia induction under 1, 3 and 30 μM, indicating that induction and emergence from GA are not mirror image processes and likely involve different neural mechanisms (van Swinderen and Kelz, 2022). We revealed a mechanism of DRN$^{5\text{-HT}}$ neurons during

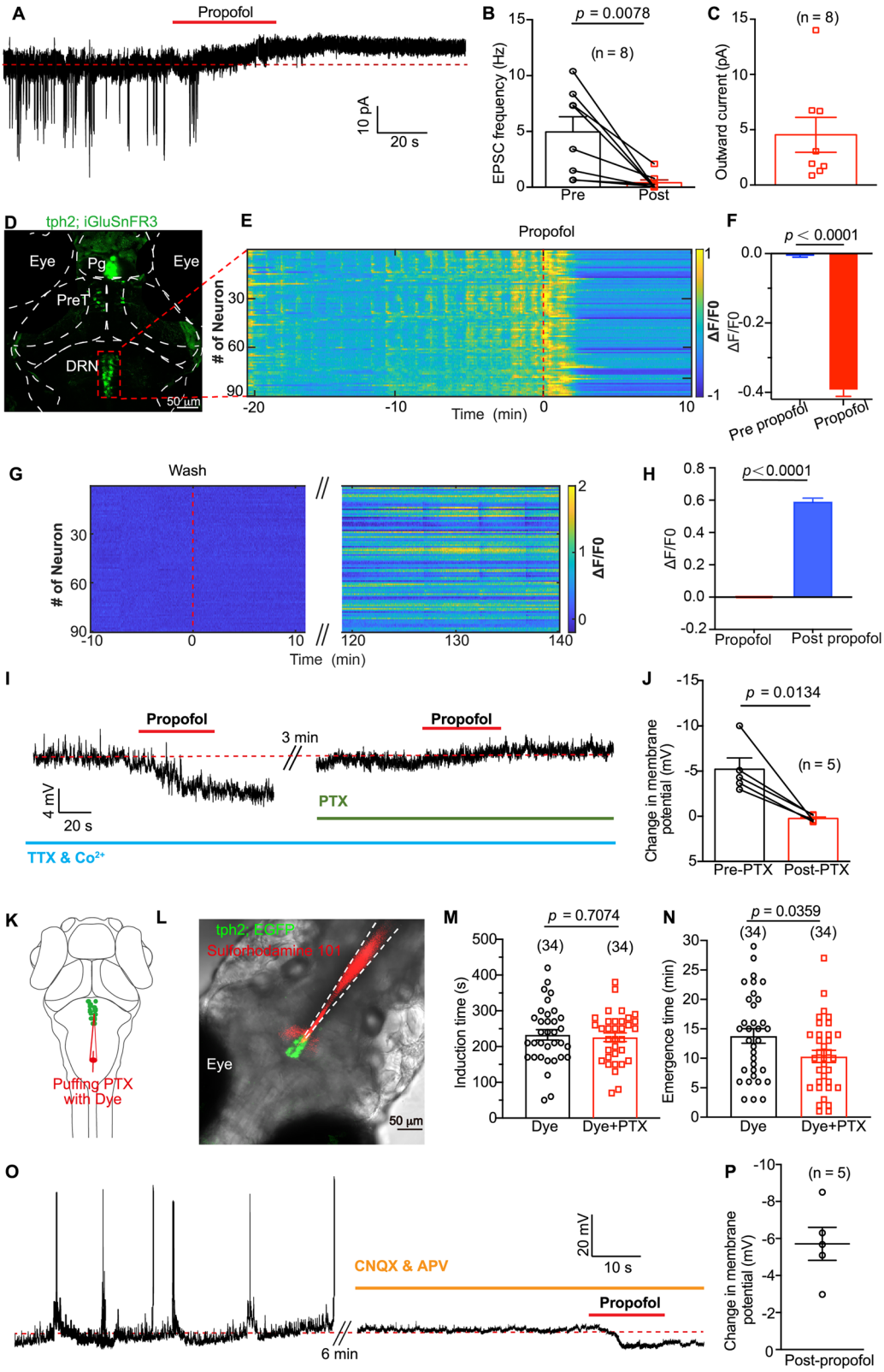

Figure 6. Propofol inhibits presynaptic excitatory glutamate inputs to DRN$^{5\text{-HT}}$ and cause membrane hyperpolarization of DRN$^{5\text{-HT}}$. ***A***, Spontaneous EPSCs of a DRN$^{5\text{-HT}}$ neuron (clamped at −60 mV) before and after puffing of propofol. The red dashed line indicates the mean leakage current before propofol application. ***B***, Summary of data showing the reduction of EPSC frequency by propofol application. Pre versus post, 4.95 ± 1.36 Hz versus 0.40 ± 0.26 Hz; $p = 0.001$; paired Student's t test. $N = 8$ cells from different larvae. ***C***, Summary of data showing the outward current induced by propofol application. $N = 8$ cells from different larvae. ***D***, Transient expression of glutamate sensor by injecting UAS, iGluSnFR3 plasmid into Ki (tph2, GAL4FF; cmlc2, EGFP) line. Pg, pineal gland; PreT, pretectum; DRN, dorsal raphe nucleus. ***E***, Representative heatmaps of glutamate events from DRN$^{5\text{-HT}}$ of one larva stimulated by dimming at 58 s interval. The red dash line indicates the timing of adding propofol to the dish. ***F***, Glutamate events were significantly inhibited by 30 μM propofol. $N = 259$ DRN$^{5\text{-HT}}$ neurons from three larvae. ***G***,***H***, iGlusnFR3 signal gradually recovered when propofol was washed by perfusion. ***I***, Representative trace showing propofol-induced membrane potential changes of a DRN$^{5\text{-HT}}$ neuron before and after application of 100 mM PTX. During the recording, synaptic transmission was blocked by replacing Ca^{2+} with Co^{2+} in the extracellular solution and adding 1 mM TTX. ***J***, Summary of data

propofol anesthesia, involving inhibition of presynaptic excitatory glutamate inputs and $GABA_A$ receptor-mediated hyperpolarization, linking the molecular mechanism of propofol with the neuronal activity of the 5-HT system.

Role of $DRN^{5\text{-}HT}$ neurons in sleep and GA

The role of 5-HT in sleep and arousal has been debated for over 50 years (McGinty, 2009). Initial studies suggested a sleep-promoting role of 5-HT neurons, but later studies supported a wake-promoting role due to the wake-active nature of $DRN^{5\text{-}HT}$ neurons. Recent studies on mice and zebrafish demonstrated the bidirectional role of the serotonergic system in sleep homeostasis and the sleep/wake cycle regulation (Oikonomou et al., 2019). The controversy may stem from the distinct effects of subpopulations of 5-HT neurons (Cheng et al., 2016; Marques et al., 2020). Most previous studies treated $DRN^{5\text{-}HT}$ neurons as a single population, but the DRN consists of subdivisions with distinct inputs, outputs, and functions (J. Ren et al., 2018), playing different or even opposite roles in various physiological responses, including light preference (Cheng et al., 2016), internal states during foraging (Marques et al., 2020), and anxiety/active coping behavior (J. Ren et al., 2018). Therefore, studying the role of $DRN5^{\text{-}HT}$ at single-cell resolution is necessary. Our study showed that functional manipulation of $DRN^{5\text{-}HT}$ neurons during propofol anesthesia promotes emergence without affecting induction under different concentrations of propofol. These results align with previous studies on inhalational anesthetics, which found that activation of $DRN^{5\text{-}HT}$ neurons promoted arousal from inhaled anesthesia without altering induction time (Li et al., 2021; Ma et al., 2023). This indicates that GA does not share exactly the same neural mechanism as natural sleep, and induction and emergence from GA are not mirror image processes (Hu et al., 2023).

General anesthetics and synaptic transmission

To confirm the effect of propofol on presynaptic excitatory inputs of $DRN^{5\text{-}HT}$ neurons, iGlusnFR3 was expressed on the extracellular surface of $DRN^{5\text{-}HT}$ neurons (the postsynaptic neurons), and the strategy was designed to visualize the presynaptic glutamate release to $DRN^{5\text{-}HT}$ neurons. Propofol completely abolished the presynaptic glutamate events of $DRN^{5\text{-}HT}$ neurons induced by dimming stimulation, as shown by a significant suppression of the fluorescence of iGluSnFR3. There are two possible reasons for the inhibition of glutamate release: propofol directly inhibits the presynaptic glutamate release or impairs the presynaptic glutamate recycle. Of note, Nicol et al. (1995) and Westphalen and Hemmings (2003) utilized l-[3H]glutamate to study the uptake of glutamate into synaptosomes at the rat cerebral cortex and reported that propofol did not affect the uptake of glutamate, which may give us a hint that the direct inhibition of the presynaptic glutamate release of $DRN^{5\text{-}HT}$ neurons could be the primary effect of propofol.

Previous in vitro evidence suggests that general anesthetics, including volatile anesthetics, propofol, and ketamine, act on synapses through both pre- (neurotransmitter release) and postsynaptic (receptor) mechanisms. Isoflurane inhibits the neurotransmitter release machinery in wild-type PC12 cells as well as hippocampal neurons (Herring et al., 2009); halothane blocks central glutamatergic synaptic transmission by presynaptically inhibiting glutamate release and postsynaptically blocking the AMPA subtype of glutamate receptors (Kirson et al., 1998); propofol and ketamine inhibit K+-evoked glutamate release from rat cerebrocortical slices by activating $GABA_A$ receptors (Buggy et al., 2000). Furthermore, in vivo evidence from Du et al. (2018) shows that propofol and etomidate suppress the locus ceruleus neuronal activities through both pre- and postsynaptic mechanisms. These data indicate the pre- and postsynaptic mechanisms of general anesthetics. Our findings suggest that propofol likely inhibits presynaptic glutamate release in $DRN^{5\text{-}HT}$ neurons and enhances postsynaptic $GABA_A$ receptor-mediated hyperpolarization.

Molecular targets of propofol

Pentameric ligand-gated ion channels (pLGICs), particularly $GABA_A$ receptors, have been extensively investigated as molecular targets for propofol. Propofol typically inhibits cation-selective pLGICs, such as nicotinic acetylcholine receptors, and potentiates anion-selective $GABA_A$Rs and glycine receptors, increasing the frequency of channel opening (Tang and Eckenhoff, 2018). Our whole-cell recording data showed that propofol induced a PTX-sensitive tonic membrane hyperpolarization of $DRN^{5\text{-}HT}$, indicating the possible existence of postsynaptic β3-containing $GABA_A$ receptors on $DRN^{5\text{-}HT}$ neurons. Propofol also targets monovalent voltage-gated ion channels, necessary for setting membrane potential and action potential propagation (Tang and Eckenhoff, 2018), and HCN channels, as demonstrated by a diminished sensitivity to propofol in HCN1− knock-out mice (Chen et al., 2009). Recent studies suggest that kinesin modulation (Bensel et al., 2017), TRPA-1 receptors (Ton et al., 2017), and SIRT-2 deacetylase (Weiser and Eckenhoff, 2015) may underlie propofol-induced unconsciousness. Further examination of membrane proteins and ion channels in $DRN^{5\text{-}HT}$ neurons is required for a full understanding of the molecular and neural circuit targets of propofol.

Limitations

There are some limitations to this study. The exact neural circuits of $DRN^{5\text{-}HT}$ neurons mediating the emergence from propofol anesthesia are still unknown and need to be identified. Additionally, 5-HT binds to diverse receptors ($5\text{-}HT_{1\text{–}7}$ receptors), including both ionotropic and metabotropic receptors, endowing the serotonergic systems with complex functions (Leopoldo et al., 2011). Future studies should explore which receptors are involved in the emergence-promoting effect of $DRN^{5\text{-}HT}$ neurons. Finally, the effect of presynaptic $GABA_A$ receptors was not studied because trans-synaptic retrograde tracking viruses have not been developed in the zebrafish model, limiting our ability to identify all presynaptic neurons of $DRN^{5\text{-}HT}$ and specifically manipulate the $GABA_A$ receptors on these neurons.

←

showing the effect of PTX on propofol-induced membrane potential changes. Without PTX versus with PTX, −5.2 ± 1.3 mV versus 0.2 ± 0.2 mV; $n = 5$; $p = 0.013$; paired Student's t test. ***K***, Schematic diagram showing local puffing of PTX with the red fluorescent dye sulforhodamine 101. ***L***, A typical case showing the area of puffing PTX with the red fluorescent dye sulforhodamine 101. ***M***, ***N***, Inhibiting $GABA_A$ receptors in DRN by local puffing PTX had no influence on induction time of propofol while significantly shortening the emergence time from propofol anesthesia (***N***, dye vs dye + PTX, 13.8 ± 1.2 min vs 10.3 ± 1.0 min; $p = 0.036$; unpaired Student's t test). ***O***, ***P***, After blocking glutamatergic receptors by adding 50 μM CNQX and 100 μM APV in the extracellular solution, local puffing of propofol caused a significant hyperpolarization of $DRN^{5\text{-}HT}$ (mean ± SEM, −5.7 ± 0.9 mV; $n = 5$ neuron). Numbers of the sample size are in parentheses.

Conclusion

We found that calcium activity of $DRN^{5\text{-}HT}$ neurons reversibly decreased during propofol perfusion. Ablation of $DRN^{5\text{-}HT}$ neurons prolonged the emergence from propofol anesthesia, while optogenetic activation strongly promoted emergence. Application of propofol to $DRN^{5\text{-}HT}$ neurons inhibited their excitability by inhibiting presynaptic excitatory glutamate inputs and inducing $GABA_A$ receptor-mediated hyperpolarization. Thus, our study indicates that the $DRN^{5\text{-}HT}$ system plays a modulatory role in the emergence from propofol GA by inhibiting the activity of $DRN^{5\text{-}HT}$ activity via $GABA_A$ receptors and blocking presynaptic excitatory glutamate inputs.

References

Aggarwal A, et al. (2023) Glutamate indicators with improved activation kinetics and localization for imaging synaptic transmission. Nat Methods 20:925–934.

Bensel BM, Guzik-Lendrum S, Masucci EM, Woll KA, Eckenhoff RG, Gilbert SP (2017) Common general anesthetic propofol impairs kinesin processivity. Proc Natl Acad Sci U S A 114:E4281–E4287.

Brian BF, Freedman TS (2021) The Src-family kinase Lyn in immunoreceptor signaling. Endocrinology 162:bqab152.

Brown EN, Lydic R, Schiff ND (2010) General anesthesia, sleep, and coma. N Engl J Med 363:2638–2650.

Brown EN, Purdon PL, Van Dort CJ (2011) General anesthesia and altered states of arousal: a systems neuroscience analysis. Annu Rev Neurosci 34:601–628.

Buggy DJ, Nicol B, Rowbotham DJ, Lambert DG (2000) Effects of intravenous anesthetic agents on glutamate release: a role for GABAA receptor-mediated inhibition. Anesthesiology 92:1067–1073.

Chen X, Shu S, Bayliss DA (2009) HCN1 channel subunits are a molecular substrate for hypnotic actions of ketamine. J Neurosci 29:600–609.

Cheng R-K, Krishnan S, Jesuthasan S (2016) Activation and inhibition of tph2 serotonergic neurons operate in tandem to influence larval zebrafish preference for light over darkness. Sci Rep 6:20788.

Collymore C, Tolwani A, Lieggi C, Rasmussen S (2014) Efficacy and safety of 5 anesthetics in adult zebrafish (*Danio rerio*). J Am Assoc Lab Anim Sci 53:198–203.

Cylinder DM, van Zundert AAJ, Solt K, van Swinderen B (2024) Time to wake up! The ongoing search for general anesthetic reversal agents. Anesthesiology 140:610–627.

Du W, Zhang R, Li J, Zhang B, Peng X, Cao S, Yuan J, Yuan C, Yu T, Du J (2018) The locus coeruleus modulates intravenous general anesthesia of zebrafish via a cooperative mechanism. Cell Rep 24:3146–3155.e3.

Franks NP (2008) General anaesthesia: from molecular targets to neuronal pathways of sleep and arousal. Nat Rev Neurosci 9:370–386.

Hemmings HC, Akabas MH, Goldstein PA, Trudell JR, Orser BA, Harrison NL (2005) Emerging molecular mechanisms of general anesthetic action. Trends Pharmacol Sci 26:503–510.

Hemmings HC, Riegelhaupt PM, Kelz MB, Solt K, Eckenhoff RG, Orser BA, Goldstein PA (2019) Towards a comprehensive understanding of anesthetic mechanisms of action: a decade of discovery. Trends Pharmacol Sci 40:464–481.

Herring BE, Xie Z, Marks J, Fox AP (2009) Isoflurane inhibits the neurotransmitter release machinery. J Neurophysiol 102:1265–1273.

Hu J-J, Liu Y, Yao H, Cao B, Liao H, Yang R, Chen P, Song X-J (2023) Emergence of consciousness from anesthesia through ubiquitin degradation of KCC2 in the ventral posteromedial nucleus of the thalamus. Nat Neurosci 26:751–764.

Jiang-Xie L-F, Yin L, Zhao S, Prevosto V, Han B-X, Dzirasa K, Wang F (2019) A common neuroendocrine substrate for diverse general anesthetics and sleep. Neuron 102:1053–1065.e4.

Kirson ED, Yaari Y, Perouansky M (1998) Presynaptic and postsynaptic actions of halothane at glutamatergic synapses in the mouse hippocampus. Br J Pharmacol 124:1607–1614.

Leopoldo M, Lacivita E, Berardi F, Perrone R, Hedlund PB (2011) Serotonin 5-HT7 receptor agents: structure-activity relationships and potential therapeutic applications in central nervous system disorders. Pharmacol Ther 129:120–148.

Li A, et al. (2021) Dorsal raphe serotonergic neurons promote arousal from isoflurane anesthesia. CNS Neurosci Ther 27:941–950.

Li J, Zhang B, Ren Y, Gu S, Xiang Y, Du J (2015) Intron targeting-mediated and endogenous gene integrity-maintaining knockin in zebrafish using the CRISPR/Cas9 system. Cell Res 25:634–637.

Lillesaar C, Stigloher C, Tannhäuser B, Wullimann MF, Bally-Cuif L (2009) Axonal projections originating from raphe serotonergic neurons in the developing and adult zebrafish, *Danio rerio*, using transgenics to visualize raphe-specific pet1 expression. J Comp Neurol 512:158–182.

Luo T, Leung LS (2011) Involvement of tuberomamillary histaminergic neurons in isoflurane anesthesia. Anesthes 115:36–43.

Luo T-Y, et al. (2020) Basal forebrain cholinergic activity modulates isoflurane and propofol anesthesia. Front Neurosci 14:559077.

Luppi AI, et al. (2023) In vivo mapping of pharmacologically induced functional reorganization onto the human brain's neurotransmitter landscape. Sci Adv 9:eadf8332.

Ma H, et al. (2023) The states of different 5-HT receptors located in the dorsal raphe nucleus are crucial for regulating the awakening during general anesthesia. Mol Neurobiol 60:6931–6948.

Marques JC, Li M, Schaak D, Robson DN, Li JM (2020) Internal state dynamics shape brainwide activity and foraging behaviour. Nature 577:239–243.

McGinty DT (2009) Serotonin and sleep: molecular, functional, and clinical aspects. Sleep 32:699–700.

Meara JG, et al. (2015) Global surgery 2030: evidence and solutions for achieving health, welfare, and economic development. Lancet 386:569–624.

Melonakos ED, Siegmann MJ, Rey C, O'Brien C, Nikolaeva KK, Solt K, Nehs CJ (2021) Excitation of putative glutamatergic neurons in the rat parabrachial nucleus region reduces delta power during dexmedetomidine but not ketamine anesthesia. Anesthesiology 135:633–648.

Mukaida K, Shichino T, Koyanagi S, Himukashi S, Fukuda K (2007) Activity of the serotonergic system during isoflurane anesthesia. Anesth Analg 104:836–839.

Muto A, Lal P, Ailani D, Abe G, Itoh M, Kawakami K (2017) Activation of the hypothalamic feeding centre upon visual prey detection. Nat Commun 8:15029.

Nicol B, Rowbotham DJ, Lambert DG (1995) Glutamate uptake is not a major target site for anaesthetic agents. Br J Anaesth 75:61–65.

Oikonomou G, Altermatt M, Zhang R, Coughlin GM, Montz C, Gradinaru V, Prober DA (2019) The serotonergic raphe promote sleep in zebrafish and mice. Neuron 103:686–701.e8.

Olsen RW, Sieghart W (2009) GABAA receptors: subtypes provide diversity of function and pharmacology. Neuropharmacology 56:141–148.

Orser BA, Bertlik M, Wang LY, MacDonald JF (1995) Inhibition by propofol (2,6 di-isopropylphenol) of the N-methyl-D-aspartate subtype of glutamate receptor in cultured hippocampal neurones. Br J Pharmacol 116:1761–1768.

Qiu G, Wu Y, Yang Z, Li L, Zhu X, Wang Y, Sun W, Dong H, Li Y, Hu J (2020) Dexmedetomidine activation of dopamine neurons in the ventral tegmental area attenuates the depth of sedation in mice. Anesthesiology 133:377–392.

Quinlan JJ, Homanics GE, Firestone LL (1998) Anesthesia sensitivity in mice that lack the beta3 subunit of the gamma-aminobutyric acid type a receptor. Anesthesiology 88:775–780.

Reitz SL, Wasilczuk AZ, Beh GH, Proekt A, Kelz MB (2021) Activation of preoptic tachykinin 1 neurons promotes wakefulness over sleep and volatile anesthetic-induced unconsciousness. Curr Biol 31:394–405.e4.

Ren J, et al. (2018) Anatomically defined and functionally distinct dorsal raphe serotonin sub-systems. Cell 175:472–487.e20.

Ren S, et al. (2018) The paraventricular thalamus is a critical thalamic area for wakefulness. Science 362:429–434.

Robinson DH, Toledo AH (2012) Historical development of modern anesthesia. J Invest Surg 25:141–149.

Roizen MF, White PF, Eger EI, Brownstein M (1978) Effects of ablation of serotonin or norepinephrine brain-stem areas on halothane and cyclopropane MACs in rats. Anesthesiology 49:252–255.

Tang P, Eckenhoff R (2018) Recent progress on the molecular pharmacology of propofol. F1000Res 7:123.

Teraoka H, et al. (2004) Hedgehog and Fgf signaling pathways regulate the development of tphR-expressing serotonergic raphe neurons in zebrafish embryos. J Neurobiol 60:275–288.

Ton HT, Phan TX, Abramyan AM, Shi L, Ahern GP (2017) Identification of a putative binding site critical for general anesthetic activation of TRPA1. Proc Natl Acad Sci U S A 114:3762–3767.

van Swinderen B, Kelz MB (2022) Anesthesia: synaptic power failure. Curr Biol 32:R781–R783.

Wang D, Guo Y, Li H, Li J, Ran M, Guo J, Yin L, Zhao S, Yang Q, Dong H (2021) Selective optogenetic activation of orexinergic terminals in the basal forebrain and locus coeruleus promotes emergence from isoflurane anaesthesia in rats. Br J Anaesth 126:279–292.

Weiser BP, Eckenhoff RG (2015) Propofol inhibits SIRT2 deacetylase through a conformation-specific, allosteric site. J Biol Chem 290:8559–8568.

Westphalen RI, Hemmings HC (2003) Effects of isoflurane and propofol on glutamate and GABA transporters in isolated cortical nerve terminals. Anesthesiology 98:364–372.

Yang X, et al. (2018) High-throughput screening in larval zebrafish identifies novel potent sedative-hypnotics. Anesthesiology 129:459–476.

Yang X, Jounaidi Y, Mukherjee K, Fantasia RJ, Liao EC, Yu B, Forman SA (2019) Drug-selective anesthetic insensitivity of zebrafish lacking γ-aminobutyric acid type a receptor β3 subunits. Anesthesiology 131:1276–1291.

Yao Y, Li X, Zhang B, Yin C, Liu Y, Chen W, Zeng S, Du J (2016) Visual cue-discriminative dopaminergic control of visuomotor transformation and behavior selection. Neuron 89:598–612.

Yin L, Li L, Deng J, Wang D, Guo Y, Zhang X, Li H, Zhao S, Zhong H, Dong H (2019) Optogenetic/chemogenetic activation of GABAergic neurons in the ventral tegmental area facilitates general anesthesia via projections to the lateral hypothalamus in mice. Front Neural Circuits 13:73.

Zhang Y, Gui H, Duan Z, Yu T, Zhang J, Liang X, Liu C (2021) Dopamine D1 receptor in the nucleus accumbens modulates the emergence from propofol anesthesia in rat. Neurochem Res 46:1435–1446.